ISTITUTO NAZIONALE DI FISICA NUCLEARE

Sezione di Genova

INFN/AE-95/19
12 Ottobre 1995

L. Rossi:

PERSPECTIVES IN HIGH ENERGY PHYSICS INSTRUMENTATION

Invited talk at the
XXIII Int. Meet. on Fundamental Physics
Comillas, Spain, May 22–26, 1995

SIS–Pubblicazioni
dei Laboratori Nazionali di Frascati

INFN - Istituto Nazionale di Fisica Nucleare
Sezione di Genova

INFN/AE-95/19
12 Ottobre 1995

PERSPECTIVES IN HIGH ENERGY PHYSICS INSTRUMENTATION

L. Rossi*
INFN–Sezione di Genova and Università di Genova, via Dodecaneso 33, I–16146 Genova

Abstract

The discovery potential of the next generation of particle accelerators, and in particular of the Large Hadron Collider (LHC), can only be fully exploited by very sophisticated particle detectors. The basics of detectors for momentum and energy measurement is here presented together with a recollection of recent developments which are relevant for use at high luminosity accelerators.

1. Introduction

The field of elementary particle detectors is wide and it evolves rapidly. Try to fit a complete description in one hour talk may turn out to be frustrating both for the speaker and for the audience. I have therefore decided to limit the presentation to few detectors which I consider representative of two classes: the momentum measurement devices and the energy measurement devices. These devices allow to determine the particles four-vector and then study the kinematics of the reactions under scrutiny. The interested reader may find a good and exhaustive description of the most widely used particle detectors in a book edited by Tom Ferbel [1].
In my talk I'll give special attention to those characteristics (space accuracy, dynamic range, granularity, pattern recognition capability, time resolution, etc.) which are crucial to better cope with the large momenta, the high multiplicity and the high interaction rate expected at the LHC.
The description of the detectors will be pedagogical, starting from the principle of operation to the most recent R&D results. Whenever convenient the historical evolution of a particle detector concept will be underlined.

2. Momentum measuring devices

Particle momenta are deduced from the formula

$$p \cos \lambda = 0.3 z B R \qquad (1)$$

* E-mail: rossi@genova.infn.it

which relates the radius of curvature R [m] and the pitch angle λ of the helicoidal track of charge z in a uniform magnetic field B [T] to the track momentum p [GeV/c]. To measure a track momentum one must therefore measure enough points on a track to recognize the track itself and then measure its trajectory. The number of space points to be measured depends on the uniformity of the magnetic field and on the topologies of the events one intends to study. The problem of momentum mesurement is therefore reduced to the problem of measuring space points with minimum perturbation to the particle trajectory.

A charged particle which crosses a medium continuously looses energy through electromagnetic interactions with the atomic electrons of the medium itself. These interactions are numerous, but the energy transfer per interaction is quite small and produces excitation and ionization of the atoms of the medium. The average energy loss is described by the Bethe-Bloch formula [2] which is valid in the hypothesis that the mass of the traversing charged particle is much larger than the electron mass:

$$-\delta E/\delta x = kz^2\beta^{-2}[\ln(2m_e c^2\beta^2/((1-\beta^2)I) - \beta^2] \qquad (2)$$

where x is the thickness of traversed material [g/cm^2], k depends on the medium (essentially on the ratio of the atomic and mass number of the material), z is the charge of the traversing particle (in units of the electron charge), β is the particle speed in units of c and I is an effective atomic ionization potential which ranges from 1 keV in lead to 13.5 keV in hydrogen. The average energy has a characteristic dependence on the velocity of the incident particle with a minimum at $\beta\gamma \approx 4$, as shown in figure 1. At this value we speak of Minimum Ionizing Particles (MIPs).

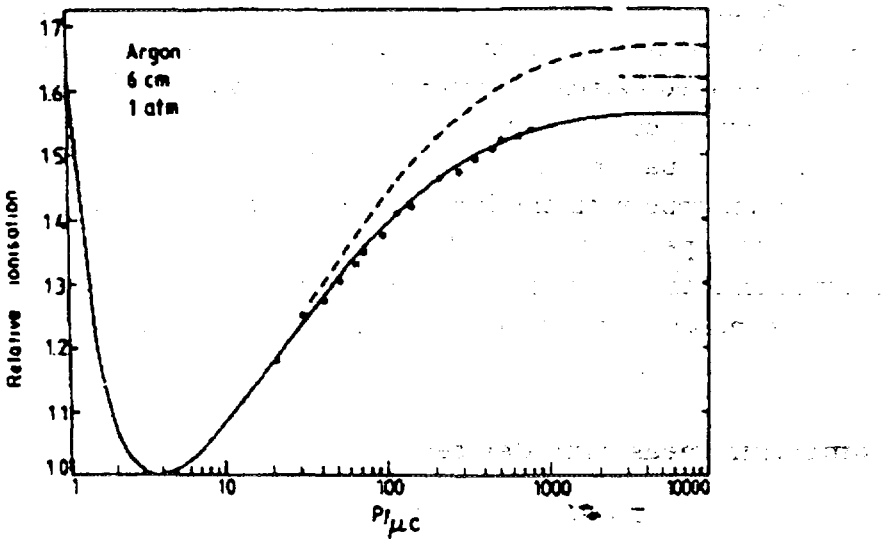

Fig. 1. Mean energy loss for a charged particle in Argon versus $\beta\gamma$

It is useful to remember that the energy loss of a MIP is about 2 MeV per (g/cm^2). If this value is compared with the mean energy necessary to liberate a pair of charge

carriers in a semiconductor (typically 3 eV) or in an insulator (typically 30 eV) we can see that to obtain a charge of 4 fC one would either need 0.3 mm of Silicon or 2.5 m of Argon at atmospheric pressure. I have choosen as an example 4 fC since this is a charge that can easily (i.e with S/N$\gg$10) be detected with present day solid state amplifiers, provided the capacitance of the detector element is low enough ($\approx$10-100 pF). A thin semiconductor layer can therefore be used to detect the passage of a MIP, a gaseous detector may, on the contrary, be used only if the charge initially released is multiplied inside the gas. The multiplication of primary ionization can happen under the action of a sufficiently high electric field. I will now discuss charge multiplication in gases and the detectors which use this process.

2.1. Gaseous position detectors

The cylindrical geometry is best suited to multiply the charge. The electric field E in a cylindrical counter (see figure 2) goes as V/r, where V is the voltage applied between the electrodes and r the distance from the center of the cylinder. Using thin ($\approx$20 μm diameter) wires as anodes, E can easily be made strong enough to start multiplication.

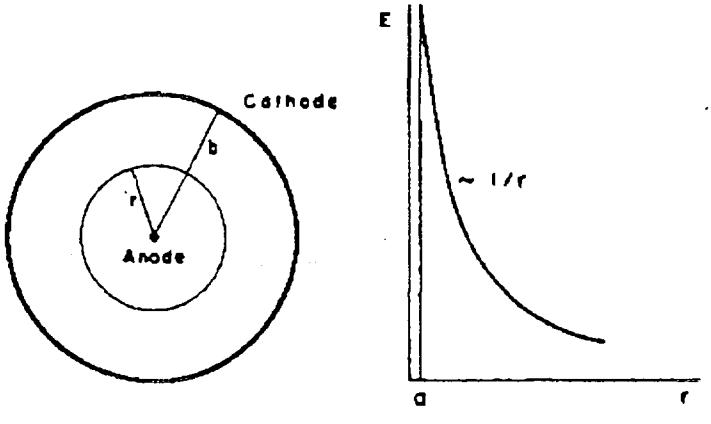

Fig. 2. Geometry of a cylindrical counter and electric field radial dependence

The multiplication happens because the electrons, which are drifting toward the anode, gain enough energy in a mean free path to ionize the gas atoms. Gains as high as 10^5 can be obtained in stable operating conditions (but the proportionality between the primary ionization and the multiplied charge can only be mantained at gains $\leq 10^4$).

The multiplication happens in the last few wire radii close to the anode as illustrated in figure 3 and takes less than 1 ns. The signals (negative on the anode and positive on the cathode) are induced by the movement of the charge through the voltage drop which will be traversed by the carriers before collection at the electrode.

The contribution of the electrons to the total signal is therefore very small (few %)

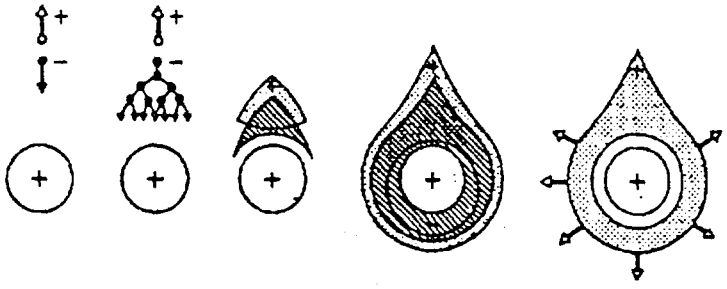

Fig. 3. Pictorial view of charge drift and multiplication in a cylindrical geometry. Time moves from left to right, dark shadow indicates electron cloud, light dark indicates ion cloud [3]

while the positive ions, which are generated far from the collecting electrode, must cross the entire cylinder and therefore induce most of the signal. The time distribution of the signal, see figure 4, shows a long tail due to the slow ion drift. Proper choice of the front-end amplifier characteristics allows to use only the very fast ($\approx$ 100 ns) component of the induced pulse.

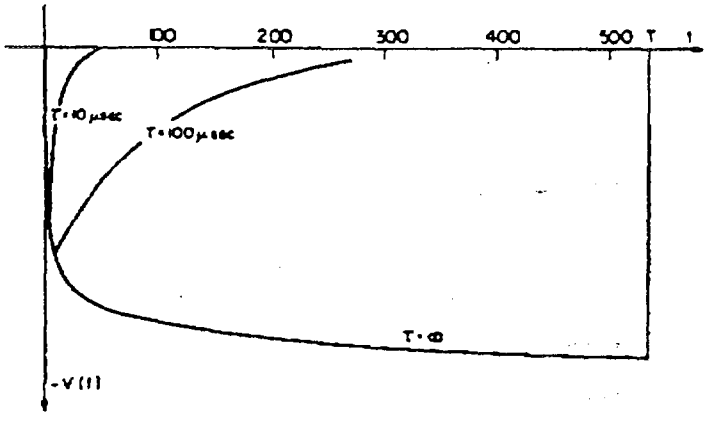

Fig. 4. Time development of the induced pulse in a proportional counter. The pulse shape obtained with various differentiation time constants is also shown [3]

The ions stay inside the detector for hundreds of microseconds and the space charge eventually built up as a consequence of a high particle flux creates an electric field that can deteriorate or stop the operation of a proportional counter. This effect depends on the geometry of the detector and on the sensitivity of the front end electronics, more details on this effect will be given later.
Cylindrical proportional counters have been widely used whenever the measurement of the energy loss was required. Today the accent is more on pattern recognition capabilities, on simplicity of construction and on minimal material along the track. Small diameter cylindrical counters with kapton foil cathodes (straw tubes [4]) arranged in matrices with large number of individual detectors have been choosen by the LHC experiment ATLAS [5] to measure tracks at distances larger than 60 cm from the interaction point.

This kind of detector has not only good pattern recognition properties, provided the occupancy is kept below 10-20%, but can also help in particle identification using the transition radiation effect [6]. Transition radiation photons are generated by the passage of ultrarelativistic particles through a medium where there are many interfaces between two materials of different dielectric constant, e.g. foam or thin plastic foils placed in between the straw tubes. The detection of these photons is possible when $\gamma \geq 1000$, this happens in most practical applications only for electrons. In this case the typical transition photon energy is ≈ 5 keV while the energy release by a MIP in a straw tube is ≈ 1 keV. The pulse height analysis of the signals given by a matrix of 64 (along the beam direction) x 12 straw tubes has allowed to identify electrons with 90% efficiency and a rejection factor against pions of about 500 [4].

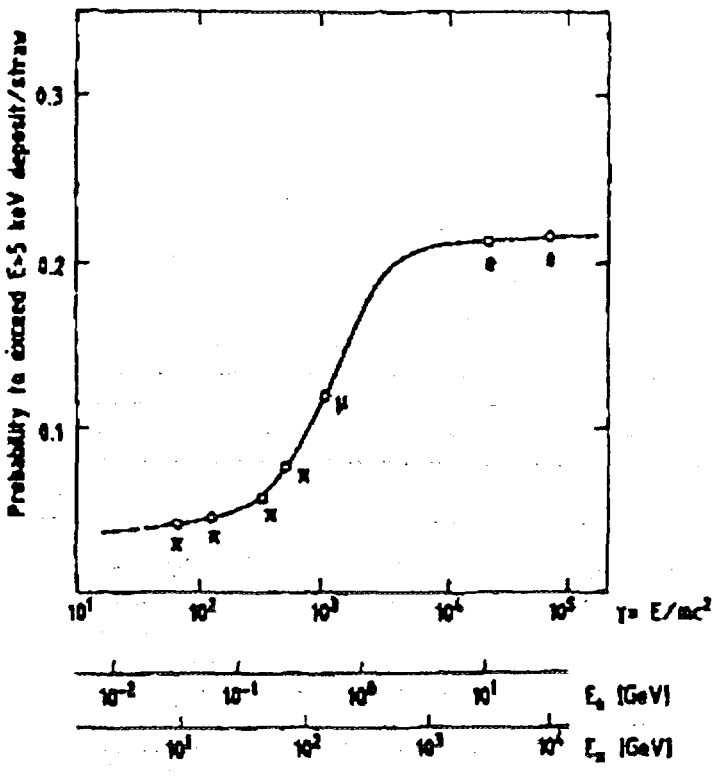

Fig. 5. Probabilty to deposit E≥ 5 keV in a 4mm diameter straw tube filled with 70%Xe + 20%CF_4 + 10% CO_2 as a function of γ

Figure 5 shows the calculated and measured probabilty to exceed, in a 4 mm diameter straw tube, the 5 keV threshold as a function of the Lorentz boost.
A very important role for the development of high energy physics has been played by the multiwire proportional counters [7] (MWPC). A MWPC consists of a set of thin, parallel and equally spaced anode wires, symmetrically sandwiched between two cathode planes. A scheme of a MWPC and the electric field equipotentials which result applying the working voltage between the anodes and the cathodes are shown in

figure 6. This extension of the proportional counter concept from the cylindrical to the multicylindrical geometry was made possible by the understanding that the positive pulse induced on the electrodes surrounding the anode interested by an avalanche largely compensates the negative signals due to the capacitive coupling of parallel unscreened wires. Each anode wire is then acting as an independent detector and the case of two contiguous wires responding is only due to the contribution of δ-rays.

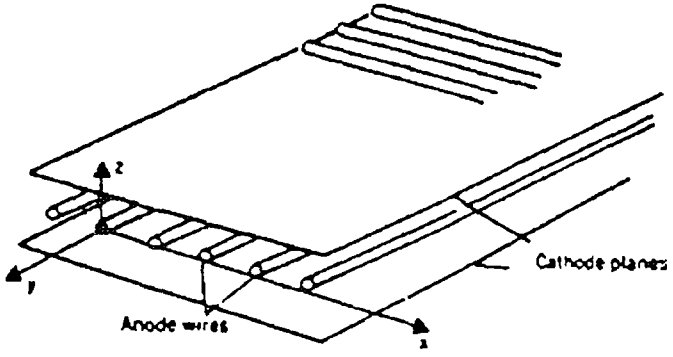

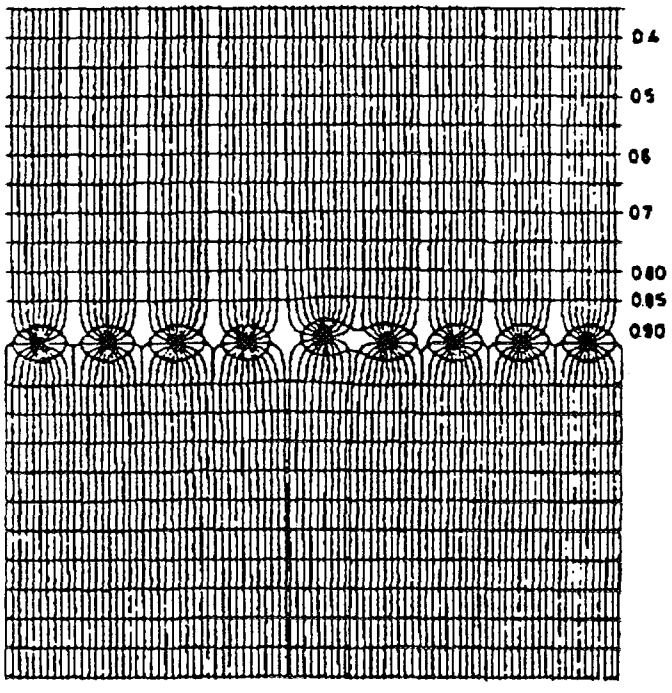

Fig. 6. Electric field equipotentials and field lines in a MWPC. The effect on the field of a small displacement of a wire is also shown [8].

The positive induced pulses are also useful to obtain an independent position measurement through charge center of gravity calculation. Properly segmenting the cathodes, as shown in figure 7, one can then obtain the two coordinates of the avalanche in the plane of the detector.

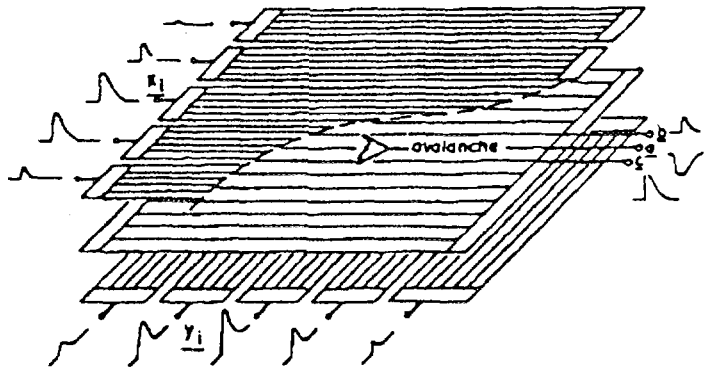

Figure 13 Principle of the center-of-gravity localization method by read-out of the induced charges on cathode planes (43).

Fig. 7. Principle of the center of gravity localization method by read-out of the induced charge on cathode planes [9]

MWPCs have been widely used in particle physics thanks to their many good characteristics: they are fast ($\approx$ 100 ns), provide good space ($\approx$ 0.5 mm) and time ($\approx$ 10 ns) accuracy, allow for large sensitive area ($\leq$ 10 m^2) with good granularity (typically 1 wire/2 mm).
It should also be stressed that an important reason for the success of the MWPC was the development of simple front end electronics, which was one of the spin-off of the more general progress of integrated circuits.
If better space accuracy ($\approx$ 0.1 mm) is needed it is possible to exploit the fact the electrons *first* drift and *then* get multiplied very close to the anode. Using an external time reference signal (given, for instance, by a scintillator), the delay between the external signal and the arrival of the electrons on the anode can be translated into a distance (drift distance) once the electron drift velocity is known.
This is, in brief, the principle of operation of the drift chambers. Typical drift cells 5 to 10 cm long are used, even if , with careful choice of gas filling and, in particular, with the minimization of the electronegative impurities at the 10^{-6} level, electrons can drift for much longer distances ($\approx$ 1 m) without appreciable losses.
Drift distance larger than 1 m are exploited in the Time Projection Chamber [TPC] [10]. This detector is the most sophisticated evolution of the drift chamber concept. It usually consists of a large drift volume ($\leq$ 10 m^3) limited on one end by an electrode at large negative voltage and on the other end by a proportional chamber with bidimensional read out.
The way the detector operates is illustrated in figure 8: the particle trajectory is projected onto the bidimensional MWPC by the electron drift. Three dimensional track information with high granularity is obtained using the timing information of each track segment read-out on the end-cap MWPC. Ion feedback prevents the use of this detector at high luminosity.

At low luminosity, as for instance at the Cern e^+e^- collider LEP, this detector

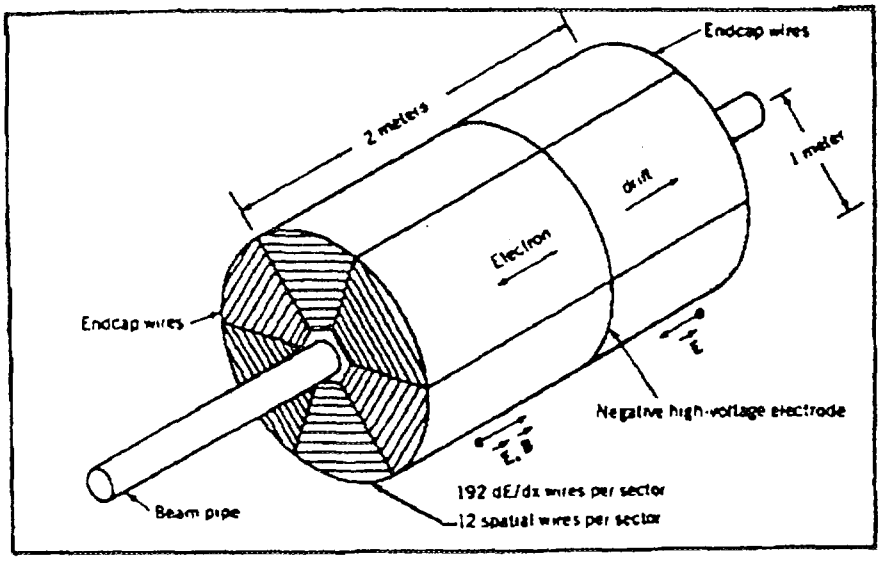

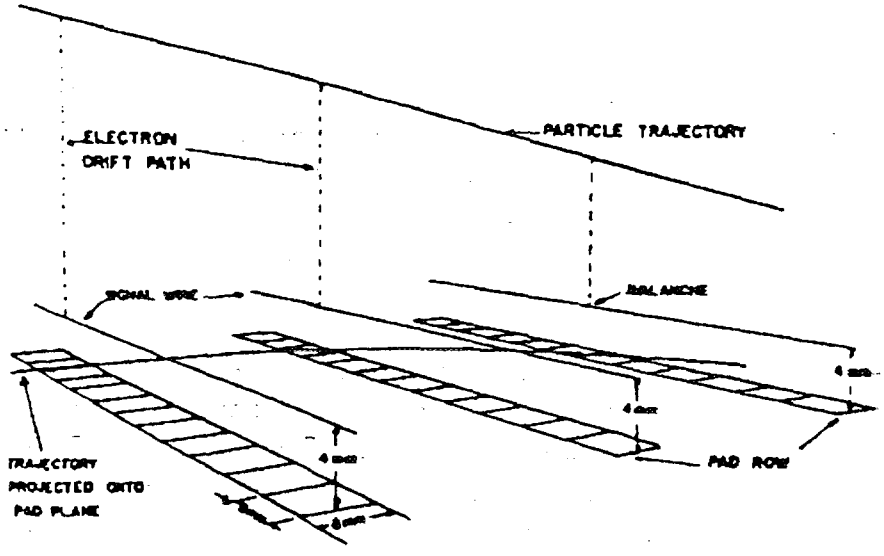

Fig. 8. Sketch of a Time Projection Chamber and of its operating principle

turned out to be extremely powerful, both for the space accuracy reached ($\approx$ 150 μm in the track bending plane) and for the pattern recognition capabilities, and there is no recent High Energy Physics conference where TPC displays of LEP events are not shown.

The new promising member of the large family of gaseous position detectors is the Micro Strip Gas Chamber [11] (MSGC). In this device the anodes and the cathodes, which are etched on the same insulating substrate through photolytographic methods, can be very close ($\approx$ 100 μm), as shown in figure 9. The primary ionization, released between the drift electrode and the cathode/anode substrate, is moved by the drift field and then multiplied in the vicinity of the anode.

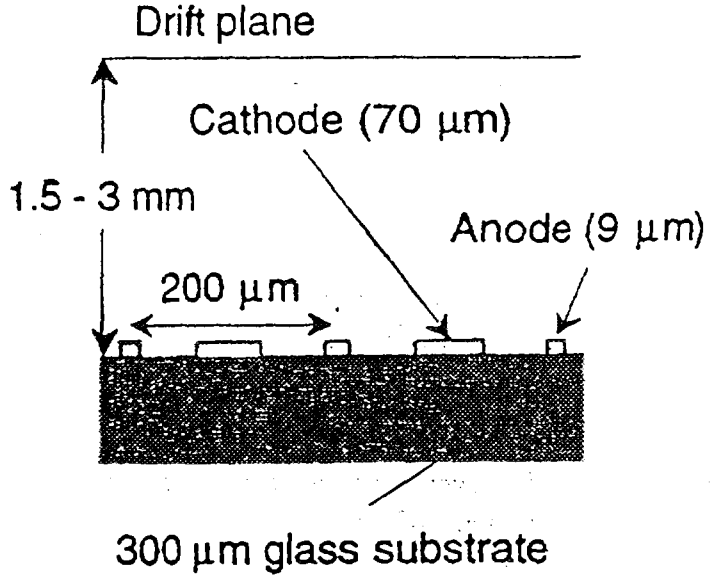

Fig. 9. Electrode configuration of a MSGC

This electrode configuration offers two major advantages: a good space accuracy ($\approx$ 50 μm) and the capability to work at very high rates since the ions of the avalanhce should only move few hundred microns before reaching the cathode. Care should be taken to the choice of the substrate resistivity in order to avoid charge-up due to trapping of ions on the surface of the insulator. A substrate resistivity of $\approx 10^9$ Ω cm allows to reach a rate of $\approx 10^6$ particles per (mm^2/s), as shown in figure 10, i.e. 2 orders of magnitude larger rate than in MWPC.

These characteristics make the MSGC suitable to measure tracks in the LHC harsh environment. The CMS [13] collaboration proposes to base the tracking inside the solenoidal magnet on a large MSGC system ($\approx 10^7$ channels). Many configurations of MSGCs have been thoroughly tested in laboratory and the study of the most important parameters has been vigorously pursued [12]. The running experience in real experiments is however still scarce, and some long term problem may still be hidden.

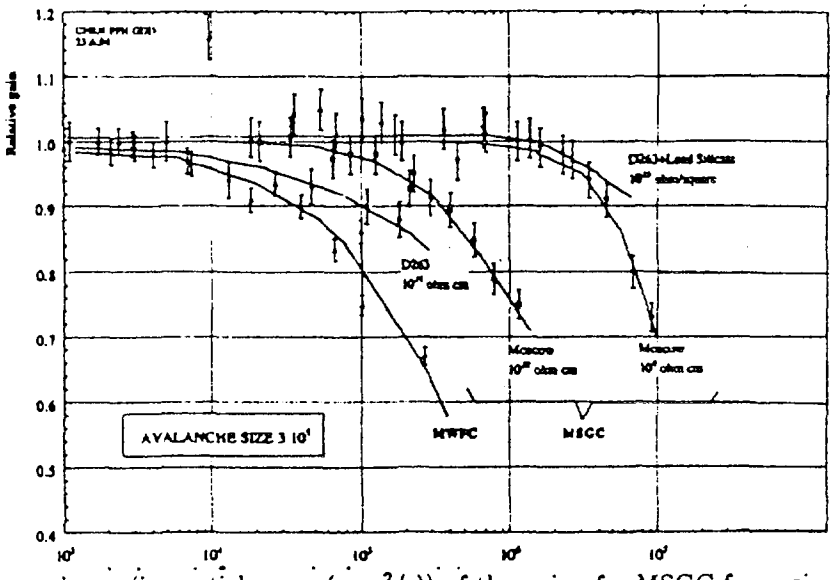

Fig. 10. Rate dependence (in particles per (mm^2/s)) of the gain of a MSGC for various substrate resistivities

As an example we show in figure 11 that the operation of a MSGC is very sensitive to the presence of polluants in the gas mixture. The useful lifetime of the detector can increase by large factors if plastic materials are avoided in the gas system.

2.2. Solid state position detectors

Very low energy is required to overcome the Fermi level in a semiconductor: ≈ 8000 carriers are produced by a MIP per 100 μm of silicon. If the silicon is doped to make a junction, we can inversely polarize this diode and a negligible current should pass through it. When a charged particle crosses the diode a small (≈ 0.5 μA on 300 μm thick fully depleted silicon) but detectable current is produced by the movement of the carriers which are liberated by the ionization process. Silicon Microstrip Detectors [14] (SMDs) are long ($\approx$ 1-10 cm) and thin ($\approx$ 10-50 μm) diodes implanted on a thin ($\approx$ 150-300 μm) high resistivity Si wafer; each of the diodes (or microstrips) acts as an independent detector.
The signals due to the ionization are quite fast ($\approx$ 10 ns) thanks to the high mobility of the carriers (1500 [600] $cm^2V^{-1}s^{-1}$ for electrons [holes]) and the high electric field (up to 10^4 V/cm) which can be applied to the high resistivity (i.e. low doping density) silicon.

Both carriers can be used and two coordinates can be read out of a single detector layer, using electrodes both on the junction and on the ohmic side, as shown in figure 12
Accuracies of $\approx$ 2 μm have been obtained [15] and several large systems have been successfully operated in fixed target and colliding beam experiments.
Short living relativistic particles decays produce tracks missing the production vertex

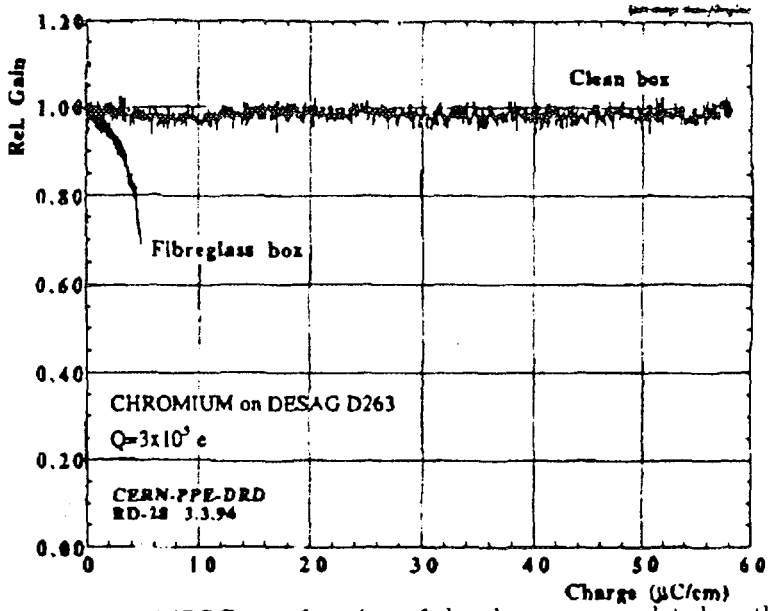

Fig. 11. Gain variation in a MSGC as a function of the charge accumulated on the electrode. Two different gas system have been used: a clean gas system made of inox (upper curve) and a gas system containing plastic and fibreglass (lower curve)

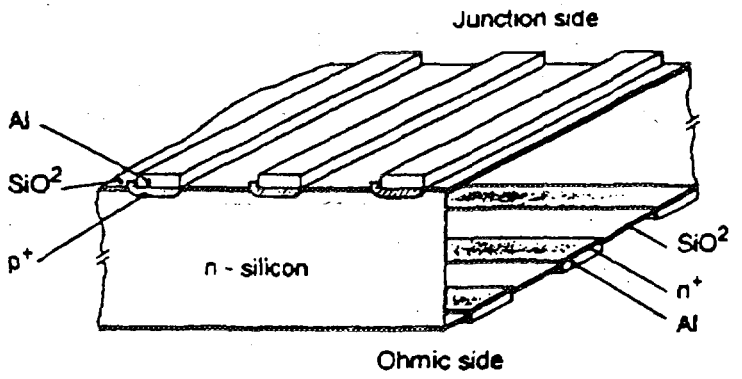

Fig. 12. Sketch of a double sided microstrip detector

by typically $c\tau$, were τ is the lifetime of the particle. SMDs could therefore detect secondary vertices of particles living a fraction of picosecond, and they have proven to be crucial to extract the signal of charm and beauty hadrons, expecially in hadronic interactions.
One other advantage of SMDs is the absence of space charge effects and therefore the capability to work at very high particle fluxes. This, together with the large number of channels per unit area, make SMDs ideal detectors for tracking at LHC close to the interaction region. The expected dose after 10 years of LHC operation causes radiation damage to the silicon and prevents the use of SMDs below a radius of $\approx$ 30 cm.
Doses higher than 10 Mrad can be tolerated either by the use of substrates (like GaAs) which are more radiation hard or by reducing the thickness T of the silicon cristal, since the depletion voltage goes like T^2. As an example a 150 μm thick cristal can be depleted (and therefore operated) at 4 times the dose of the most usual 300 μm thick cristal. Thinner silicon layers can be used if the capacitance C of the detector element can be reduced, since the noise of the amplifier scales like $\sqrt{C}$.
This is the case in pixel detectors [16] [17], which can be regarded as very short ($\approx$ 0.5 mm long) strips. These detectors allow for a thousandfold increase in segmentation, as compared to SMDs, and provide the space and time accuracy of a SMD in a true 2-dimensional geometry, without matching ambiguities between projections. In order to extract the signal from the 2-dimensional pixel matrix an equivalent matrix of front end electronics should be connected to the detector.

Figure 13 shows the connection between one pixel and its read out electronics obtained through a droplet (bump) of solder or indium. Pixel detectors have been used in experiment [18] and they have shown to be a powerful tool for pattern recognition in a high multiplicity environment, thanks to the large number of cells per unit area ($2400/cm^2$) and to the very low noise (probability of spurious hit $\leq 10^{-8}$).
R&D must still be done mostly on read out architecture, on radiation hard electronics and on high density connections in order to fully exploit all the potentialities that this approach offers.
Both ATLAS [5] and CMS [13] propose to use pixels as vertex detectors; other applications in different fields, like medical diagnosis, where fast photon localization is needed are under study [19].

3. Energy measuring devices

The energy measurement I'm going to describe here is a destructive measurement, i.e. the incident particle looses all his energy , mostly through inelastic collisions, inside the detector. This kind of detector, named calorimeter [20], is the only device which can measure the energy of neutral particles, like π^0 or neutrons. It must be massive, since it should fully contain the shower developed by the incident particles,

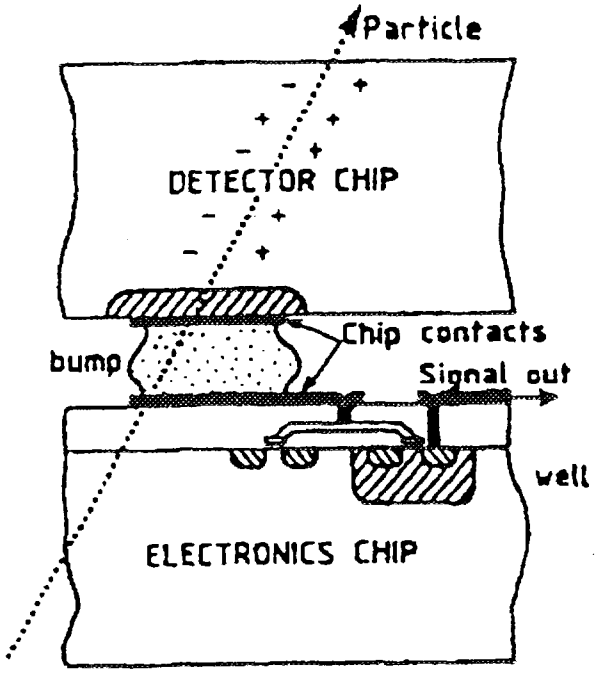

Fig. 13. A pixel detector element connected to its read out electronics

some of which may have energy of hundreds of GeV. The name calorimeter is justified by the fact that most of the incident energy is dissipated as heat. Only a tiny fraction of the energy deposited E, like scintillation or Cerenkov light or ionization charge, gives proper signal for particle detection. The height of any of these signals is proportional to the the number N of charged particles which are produced by the incident particle during its slow down process in the calorimeter (see figure 14).

Since N$\propto$E this gives:

$$\sigma(E)/E \sim \sigma(N)/N \sim 1/\sqrt{N} \sim 1/\sqrt{E} \qquad (3)$$

which indicates that the calorimeter has better energy resolution with increasing energy. This explains why these devices became more important in the last 20 years, when accelerators, producing particles of sufficiently high energy to justify the use of calorimeters, came into operation.

Calorimeters are either optimized for electromagnetic or for strong interactions, we then choose high Z [A] materials to better contain the shower and we speak of electromagnetic [hadronic] calorimeters.

The basic processes are different in the two types of calorimeter and a separate description is therefore preferable.

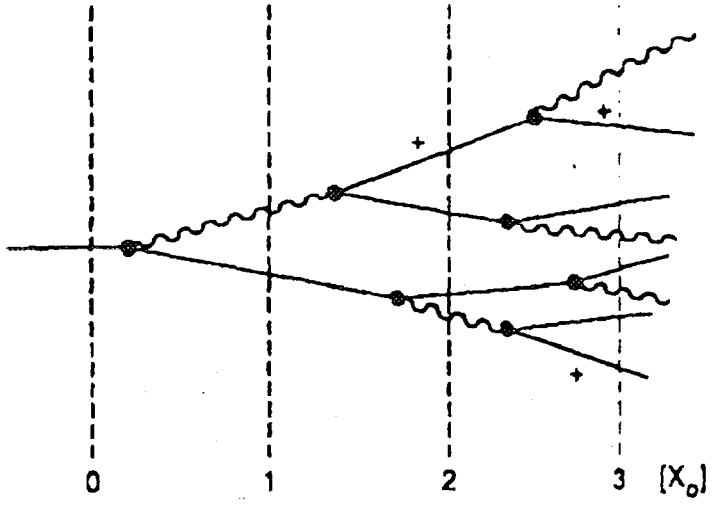

Fig. 14. Sketch of the start up of an electromagnetic showers

3.1. Electromagnetic showers

As shown in figures 15 and 16 two processes dominate the shower development for energies exceeding the critical energy ϵ ($\epsilon \sim 550/Z$ MeV). They are brehmsstralung, in case of $e^{\pm}$, and pair production in case of γ's.

The only scale which is relevant for these processes is the radiation lenght X_0, i.e. the lenght over which the energy is degraded to 1/e of its initial value. This quantity is related to the mean free path between collisions, depends on the material and, for sufficiently heavy nuclei ($Z \geq 10$), can be approximated with the formula:

$$X_0\ [g/cm^2] = 180\ A/Z^2$$

The shower development continues until the energy of the particles inside is $\geq \epsilon$. After having gone through a maximum the shower dies out in few X_0, as shown in figure 17, which also illustrates that the longitudinal shape of the shower, once expressed in units of X_0, is very similar in all materials.

The energy resolution of a calorimeter depends on the fluctuation of the "measurable" track lenght. Part of the track lenght may be unmeasurable because of threshold effects (e.g. the emission of Cherenkov light in lead glass absorbers) or because part of the material in the calorimeter is not active. While threshold effects happen for any energy deposit mechanism which can produce measurable signals, loss of track lenght in passive materials happens only in sampling calorimeters. In these devices the particle absorption and the signal extraction functions are separated. Layers of very dense material (e.g. lead), used to develop the showers, are interleaved with layers of detectors (e.g. sheets of scintillators).

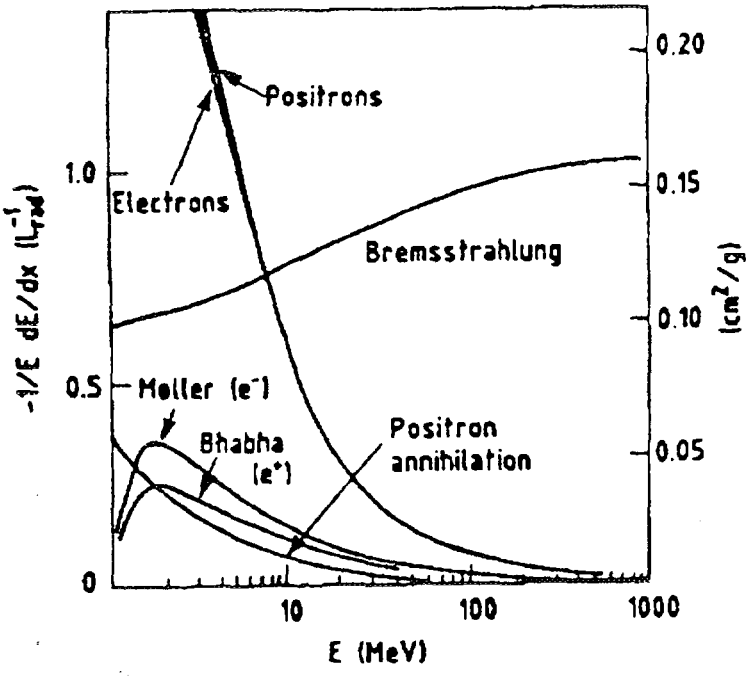

Fig. 15. Fractional energy loss per radiation lenght (left ordinate) and per g/cm^2 (right ordinate) in lead as a function of e$^\pm$ energy [1]

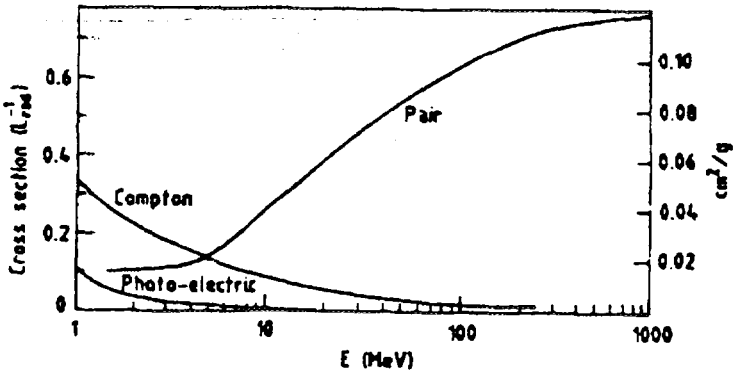

Fig. 16. Photon cross section in lead as a function of the photon energy [1]

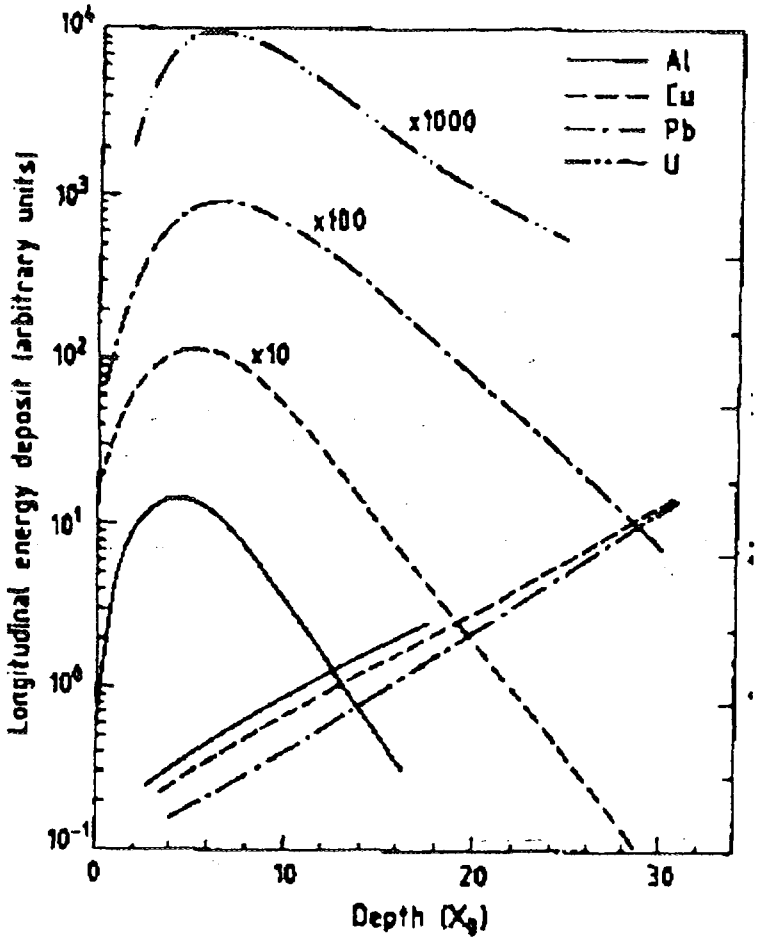

Fig. 17. Longitudinal shower development of 6 GeV electrons in Al, Cu, Pb, U, showing the scaling with the radiation lenght X_0 [1]

Homogeneous calorimeters provide typical energy resolution of

$$\sigma(E)/E \sim 0.01/\sqrt{E} + 0.01$$

while, for sampling calorimeter,

$$\sigma(E)/E \sim 0.1/\sqrt{E} + 0.01$$

The constant term is a parametrization of the complexity of these multi-ton systems and includes local non uniformities, calibration accuracy and stability and other effects. At very high energy the constant term becomes dominant and the sampling approach may be preferred for various reasons, like cost or radiation resistence or spatial accuracy.

3.2. Hadronic showers

Showering is, in this case, mostly due to hadronic collisions. These are more complicated than the electromagnetic ones, which results in a wider fluctuation of the energy deposit. Containment of hadronic showers requires large thickness of material with high atomic number and this implies that, for practical reasons, all hadronic calorimeters are of the sampling type. The purely hadronic part of the shower (70%, the rest is electromagnetic because of π^0 production) does not give detectable signal as efficiently as an electromagnetic shower, as illustrated in figure 18.

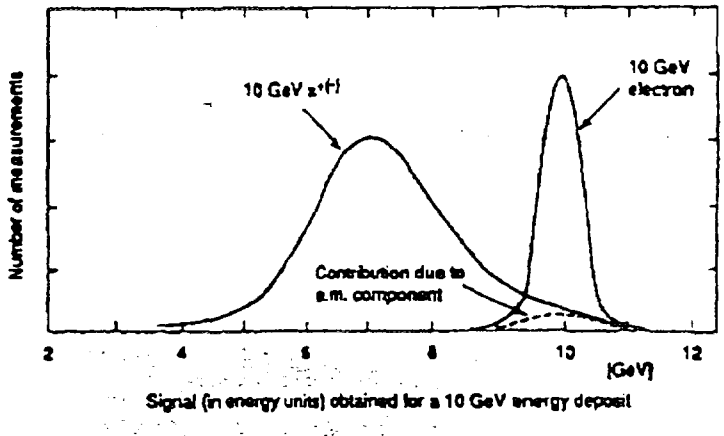

Fig. 18. Comparison of the energy deposition of a hadronic and an electromagnetic shower initiated respectively by 10 GeV $\pi^{\pm}$ and 10 GeV $e^{\pm}$ [21].

This is because part of the energy is spent to overcome the nucleon binding energy and most of the very low energy nuclear fragments cannot be detected. This deficit can be compensated using the neutrons which are in the shower to induce fission in very heavy (e.g. U) absorbers [22]. Careful choice of the read out material and of its thickness ratio to the absorber allow to have the same response for electrons and for hadrons [23] and an energy resolution of $0.2/\sqrt{E}$ can be obtained, while, for non compensating calorimeter, the resolution goes more like $0.5/\sqrt{E}$.

3.3. One example of recent development in calorimeters

Calorimeters to be used at LHC should be fast, radiation resistent and have no cracks; if they are of the electromagnetic type they should also provide good energy resolution and good space accuracy.
The liguid argon (LAr) accordion electromagnetic calorimeter [24] use a special geometry to fullfill the above requirements. The basic difference between a standard absorber/detector arrangement and the accordion layout can be understood looking at figure 19. Both layouts are based on measuring in each of the LAr layers the ionization produced by the tracks of the shower (see figure 20), each LAr layer works as an ionization chambers.

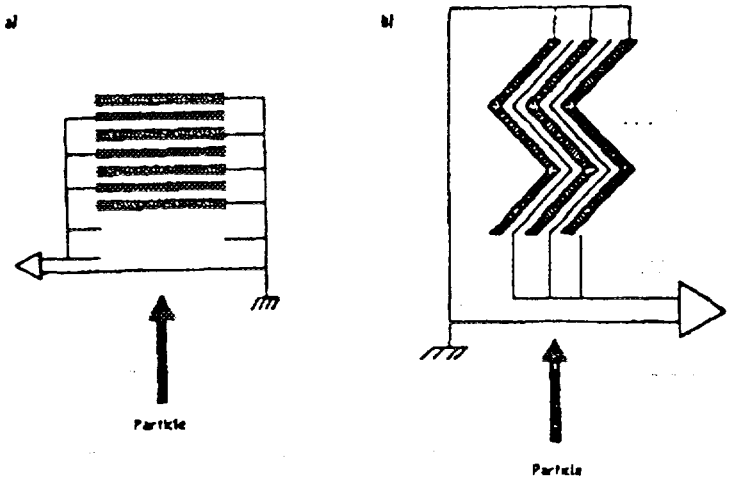

Fig. 19. Sketch of (a) the conventional and (b) the accordion absorber read-out arrangement in a LAr sampling calorimeter

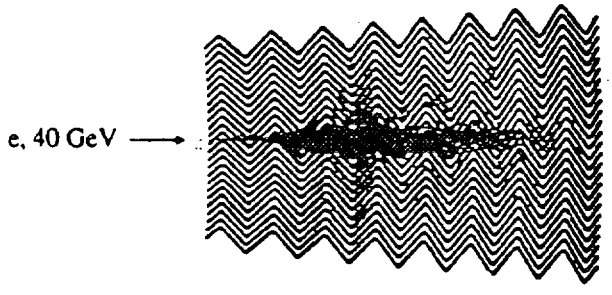

Fig. 20. Simulation of a shower inside the accordion geometry

The advantage of the accordion layout is twofold:

a) its structure can be repeated transversally to the incoming particle direction without cracks up to practical dimensions for handling;

b) the read-out of the ionization is obtained through pick-up kapton electrodes located at the centre of each LAr gap and connected to the preamplifier at the back of each accordion tower. This set up minimizes the capacitance of the transmission line to the preamplifiers and optimizes the speed of the detector.
Only one part of the ionization signal is used if high rate operation is necessary. Fast shaping of part of the triangular current pulse (see figure 21) allows to measure the total charge deposit by simple extrapolation.

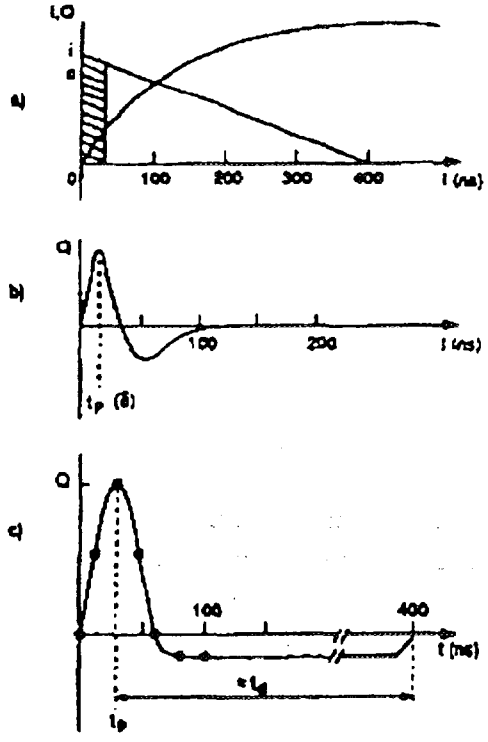

Fig. 21. Signals in a LAr calorimeter: (a) current and induced charge, (b) fast bipolar shaping and (c) the observed signal which is a convolution of (a) and (b) [21]

Drawback of the accordion geometry is the difficulty to implement longitudinal segmentation, which is necessary to measure the profile of the shower deposit along the calorimeter. This information is important to optimize the e/π separation.
Large scale prototypes of the accordion calorimeter have been built and all the basic measurements have been carried out. The energy resolution has been found to be:

$$\sigma\ (E)/E = 0.096/\sqrt{E} + 0.004$$

the space resolution, which is important for π^0 reconstruction and for matching the information provided by the calorimeter with the information of the tracking detectors, has been measured to be:

$$\sigma(x) = 5\ mm/\sqrt{E}$$

Finally, the uniformity of response, which can be a worry in this geometry, has

been measured below ~1%, as shown in figure 22.

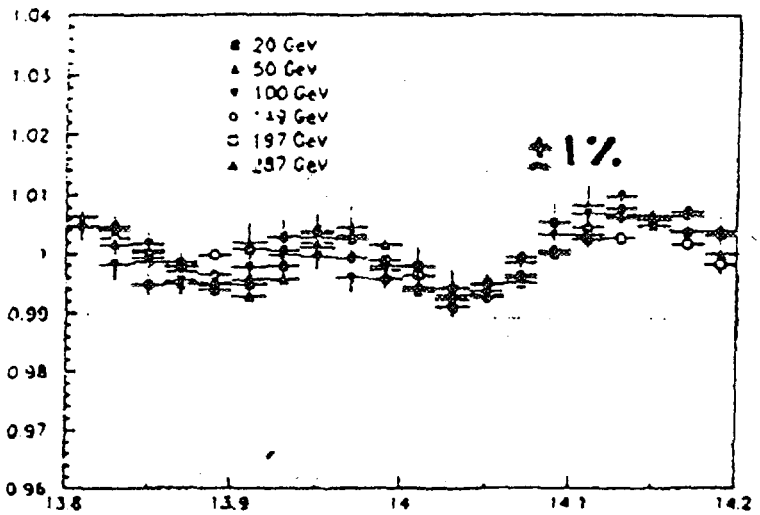

Fig. 22. Uniformity of response to electromagnetic showers of the accordion calorimeter as a function of the impact point of the incoming electron

4. Conclusions

Many recent developments in particle detectors have been driven by the very demanding needs of LHC.
A lively R&D program has been set up at Cern from 1990 to 1994 under the control of the Detector Research and Develpment Committee to find ways of better exploiting the potentialities of a high luminosity collider like the LHC.
Most of the novel results presented in this review originate from this program.

5. Aknowledgments

I am grateful to the organizers of this conference for the very kind hospitality in the enchanting atmosphere of Comillas.

6. References

1. *Experimental Techniques in High-Energy Nuclear and Particle Physics* ed. T.Ferbel, World Scientific, Singapore
2. H.A.Bethe, *Annalen der Physik* **5** (1930)325
3. *Principle of operation of multiwire proportional and drift chambers* F.Sauli, Cern Report 77-09 (1977)
4. RD-6 Collaboration, CERN/DRDC/93-46, Nov. 1993
5. Atlas Technical Proposal, CERN/LHCC/94-43, LHCC/P2, Dec. 1994
6. V.L.Ginzburg and I.M.Frank, *IETP* **16** (1946)15
7. G.Charpak et al. *Nucl. Instrum. and Methods* **62** (1968)235
8. G.A. Erskine *Nucl. Instrum. and Methods* **105** (1972)565
9. G.Charpak et al. *Nucl. Instrum. and Methods* **148** (1978)471
10. D.R.Nygren *Phys.Scripta* **23** (1981)584
11. A.Oed et al. *Nucl. Instrum. and Methods* **A263** (1988) 351
12. RD-28 Collaboration, CERN/DRDC/93-34, Sept. 1993
13. CMS Technical Proposal, CERN/LHCC/94-42, LHCC/P1, Dec. 1994
14. S.R.Amendolia et al. *Nucl. Instrum. and Methods* **176** (1980)449
    E.H.M.Heijne et al. *Nucl. Instrum. and Methods* **178** (1980)331
15. M.Adinolfi et al. *Nucl. Instrum. and Methods* **A329** (1993)117
16. E.H.M. Heijne et al. *Nucl. Instrum. and Methods* **A273** (1988) 615
17. H. Spieler *Integrated microsystems as a driving force in modern detector design* Ed. M. Budinich et al., Int. Conf. on the Impact of Digital Microelectronics and Microprocessors on Particle Physics, Trieste 28-30 March 1988 World Scientific, Singapore, 1988 1672
18. F.Antinori et al. *Nucl. Instrum. and Methods* **A360** (1995) 91
19. E.H.M. Heijne *Physica Medica* **9** (1993) 109
20. M.Atac et al. Proc. Calorimeter Workshop, FNAL, Batavia, Ill. (1975)
21. C.W.Fabjan CERN-PPE/94-61
22. C.W.Fabjan et al. *Phys. Lett.* **60B** (1975) 105
23. R.Wigmans *Nucl. Instrum. and Methods* **A265** (1988) 273
24. B.Aubert et al. (RD3 Collaboration) CERN-DRDC/90-31
    B.Aubert et al. *Nucl. Instrum. and Methods* **A324** (1992) 93